Géotechnique **00**, 1–20 [http://dx.doi.org/10.1680/geot.XX.XXXXX]

Nonlinear soil-pile interaction induced by ground settlements: pile displacements and internal forces

A. FRANZA*, A. M. MARSHALL† and R. JIMENEZ‡

In urban areas, the construction of tunnels and deep-excavations beneath and near to pile foundations can be detrimental for the superstructure and the foundation. A two-stage continuum-based nonlinear soil-pile interaction model is presented in this paper for predicting the axial and flexural response of piles affected by ground movements. The model accounts for the effects of near-pile non-linear (hyperbolic) soil stiffness degradation and unloading effects. The approach is used to analyse the relationship between the pile axial response (both displacements and internal forces) and greenfield ground settlements for purely-frictional and floating piles in uniform ground. Both displacement and non-displacement piles are analysed by applying appropriate pre-excavation loading sequences. Results demonstrate the influence of initial safety factor, installation method, and capacity distribution (between shaft and base) on pile settlements and on critical tensile axial forces (both in terms of magnitude and depth). Dimensionless design charts are provided to estimate pile settlements and critical axial forces for the case of greenfield settlements that either increase or decrease linearly with depth. These charts provide a rational and more general framework to describe excavation-induced effects on piles than empirical methods.

KEYWORDS: Tunnels & tunnelling, deep-excavations, settlement, pile, soil/structure interaction

INTRODUCTION

Engineers need to estimate the effects of ground movements resulting from tunnelling and deep-excavations (collectively referred to as *excavations* in this paper) on pile foundations. Previous research has extensively investigated the flexural response of piles to horizontal ground movements caused by urban excavations (among others, Chen *et al.* (1999); Mu *et al.* (2012); Poulos & Chen (1997); Loganathan *et al.* (2001); Zhang *et al.* (2018)) and has provided design charts for estimating lateral deflections and internal moments. On the other hand, the pile response for problems dominated by ground settlements (e.g. tunnelling beneath piles, excavations deeper than pile base level) has not yet been fully characterised (Dias & Bezuijen, 2015; Mair & Williamson, 2014).

The soil-pile interaction problem is generally studied in terms of both pile settlements (associated with distortions and damage of buildings and infrastructure) and pile axial forces (linked with potential for pile cracking). Pile settlements are related to greenfield settlements $u_{z,gf}$ (when no pile is present) using the *interaction level depth*, z_i, which defines the soil depth where greenfield soil settlement (along the pile axis) matches that of the pile. Note that the interaction level is close (but not always identical) to the neutral level, which is the depth at which the pile shaft friction changes from negative to positive (Korff *et al.*, 2016). In addition, the *critical level depth*, z_c, is defined as the depth at which the pile experiences the *critical axial force*, N_c, which is the maximum tensile or minimum compressive force along the pile after excavation (i.e. the combined result of pre-excavation pile head loading and excavation-induced ground movements). Note that, in this paper, a positive sign convention is used for tensile axial forces (e.g. $N_c > 0$ for a tensile force).

As a first approximation, when dealing with a piled structure affected by excavation-induced ground settlements, a soil-single pile interaction scenario is generally considered. This approach neglects the effects of pile-pile interactions and of pile load redistribution due to superstructure stiffness (i.e. it assumes a constant pile head load, P). For the case of urban excavations, studies have investigated qualitatively the relationship between interaction level z_i, initial pile safety factor

Manuscript received...
* ETSI Caminos, Universidad Politécnica de Madrid, Madrid, Spain. Corresponding author email: andreafranza@gmail.com
† Department of Civil Engineering, University of Nottingham, Nottingham, UK.
‡ ETSI Caminos, Universidad Politécnica de Madrid, Madrid, Spain.

$SF_0 = Q_{tot}/P$ (where $Q_{tot} = Q_b + Q_s$ is the ultimate pile capacity given by the resistance of the shaft Q_s and base Q_b), and subsurface greenfield settlements (among others, Basile (2014); Bel *et al.* (2015); Dias & Bezuijen (2018); Franza & Marshall (2019); Williamson *et al.* (2017b); Zhang *et al.* (2011b)). The interaction level is affected by the distribution of the ultimate pile capacity, which also defines the type of deep foundation: a purely-frictional pile with little base resistance, a floating pile with both shaft and base resistance, and an end-bearing pile with little shaft resistance (Mair & Williamson, 2014; Korff *et al.*, 2016). In practice, engineers commonly use design charts that relate pile head settlement to greenfield surface settlement depending on the location of the pile base (Kaalberg *et al.*, 2005; Selemetas, 2005; Selemetas & Standing, 2017), as shown in Figure 1. Alternatively, an empirical method can be used where pile settlement is taken as the greenfield settlement at (i) the surface, (ii) two-thirds the pile depth, and (iii) the pile base (i.e. z_i/L_p =0, 2/3, 1) for (i) purely-frictional, (ii) floating, and (iii) end-bearing piles, respectively (Devriendt & Williamson, 2011; Jacobsz *et al.*, 2005). This method was used during the preliminary design stages of the Crossrail project (Williamson, 2014). Both of these approaches neglect the influence of SF_0. In fact, increased service loads P (i.e. for a reduced SF_0) as well as soil non-linearity were found to increase excavation-induced pile settlements and, thus, z_i (Basile, 2014; Dias & Bezuijen, 2018; Williamson *et al.*, 2017b; Zhang *et al.*, 2011b). Korff *et al.* (2016) proposed a dimensionless framework to predict z_i that accounted for the effect of SF_o but was limited to the case of non-displacement single piles subjected to deep-excavation settlement profiles that decrease with depth. Tunnelling, however, is characterised by zones where both increasing and decreasing greenfield settlement profiles occur, as summarised in Figure 2.

The soil-pile interaction caused by ground movements also impacts pile internal forces. The main mechanisms relating to pile axial forces caused by excavation-induced ground movements have been studied (among others, Hong *et al.* (2015); Huang & Mu (2012); Kitiyodom *et al.* (2005); Loganathan *et al.* (2001); Lee & Chiang (2007); Soomro *et al.* (2015, 2017, 2019)). The excavation-induced variation of internal pile forces decreases with the magnitude of ground movements (Basile, 2014); in addition, piles with service loads approaching pile capacity with low initial safety factors suffer smaller additional excavation-induced axial forces than lightly loaded piles with high initial safety factors (Williamson *et al.*, 2017a,b; Zhang *et al.*, 2011b). In particular, there is the potential for tensile forces to develop within a pile located in the zone directly above a newly constructed tunnel (i.e. for linearly increasing greenfield ground movements), which was not considered by Korff *et al.* (2016). As discussed by Williamson (2014), pile cracking due to these tensile forces was a source of uncertainty for the field monitoring of piles affected by Crossrail tunnelling.

Finally, the construction/installation method (displacement or non-displacement piles) could impact the tunnel-pile interaction by influencing the pre-tunnelling distribution of mobilised soil reaction forces (in both undrained and drained conditions) as well as the effective stress level of the soil (in drained conditions). In particular, while displacement piles can have, prior to tunnelling, negative (downwards) friction along portions of their shaft (due to post-installation residual stresses in the soil and pile), and a base reaction force greater than the vertical service load ($Q_b > P$), non-displacement piles have positive (upwards) shaft friction mobilised throughout and a base reaction force lower than the applied service load ($P > Q_b$). Previous analytical studies mostly focused on non-displacement piles while this paper deals with both cases of displacement and non-displacement piles (referred to as *DP* and *NP*, respectively).

SCOPE

A single pile with constant head load is studied using a nonlinear-elastoplastic continuum-based model to predict the response of piles to excavation-induced ground movements (where the term *excavation* refers to both tunnelling and deep-excavations). A parametric study is carried out for greenfield settlements with linearly increasing or decreasing profiles with depth, as shown in Figure 2. Dimensionless design charts are provided for preliminary interaction assessments, describing the main parameters affecting the settlements and post-tunnelling internal forces of displacement and non-displacement piles in uniform soil.

MODEL

In this paper, a nonlinear continuum-based two-stage analysis method is adopted. The excavation is considered only in terms of induced greenfield ground movements with no change in the effective stress profile. The soil response to loading is not affected by the presence of the excavation. This is consistent with previous tunnel- and deep excavation-pile interaction analyses carried out using boundary element (BEM), finite element (FEM), and finite difference (FDM) methods adopting either continuum or Winkler mechanical models for the soil (Basile, 2014; Chen *et al.*, 1999; Franza *et al.*, 2019a; Loganathan *et al.*, 2001; Williamson *et al.*, 2017b; Korff *et al.*, 2016; Zhang *et al.*, 2011b, 2013). The soil is modelled as a homogeneous and isotropic half-space (referred to as a continuum) in which perfectly-plastic behaviour (e.g. due to slippage or soil failure) can occur at the pile-soil interface. Soil nonlinearity is assumed to be confined to the area near the pile shaft and base

(referred to as *near-pile*), while the response describing interactions between different nodes along the pile (referred to as *far-pile*) is assumed linear elastic. The initial near-pile and far-pile response of the soil to loading depends on the soil's elastic parameters (i.e. initial Young's modulus, $E_{s,0}$, and Poisson's ratio, ν_s). These are described, respectively, by the diagonal and off-diagonal terms of the flexibility matrix obtained by integrating Mindlin's solutions along the pile boundary. The near-pile response is assumed either linear-elastic perfectly-plastic (EP solution) or nonlinear elastoplastic (NEP solution), as illustrated in Figures 3a and 3b.

To achieve the EP perfectly-plastic local soil behaviour shown in Figure 3a, sliders with limit forces were added at the pile-soil interface, while a near-pile soil stiffness of $E_{s,0}$ was assumed for both loading an unloading. In the NEP method, in addition to sliders, the dependency of soil stiffness on the loading path (i.e. different stiffness for loading and unloading) and the soil stiffness degradation with relative soil-pile displacements was also considered, as displayed by Figure 3b. For loading and reverse loading, the tangent Young's modulus of the near-pile soil E_s is decreased according to the Duncan-Chang hyperbolic law for which $E_s = E_{s,0} \times \left(1 - R_f f/f_f\right)^2$, which depends on the ratio between local soil reaction forces f and the ultimate forces f_f, as well as the coefficient of hyperbolic stiffness reduction R_f, ranging between $0.8 - 1$ (Castelli & Maugeri, 2002). This law is commonly adopted to predict pile response to external loading (Castelli & Maugeri, 2002; Chow, 1986; Poulos, 1989) and has been used within other soil-pile interaction analyses (Basile, 2014; Zhang *et al.*, 2011b, 2013). For unloading-reloading (paths AB' and C'D' in Figure 3b; i.e. for load increments causing a soil stress that is less than the largest positive or negative value experienced during its history), the local stiffness is assumed equal to the initial Young's modulus $E_{s,0}$.

The effect of the hyperbolic coefficient R_f on the stiffness degradation is shown schematically in Figure 3c. As a result of the plastic sliders, the elastic perfectly-plastic behaviour EP is given by $R_f = 0$. For the NEP behaviour, an asymptotic trend associated with a negligible tangent stiffness is obtained at large deformations when $R_f = 1$, whereas a more gradual stiffness degradation is given for $R_f < 1$ up to the triggering of the slider limit force.

Finally, EP and NEP behaviour was only implemented in the vertical direction, whereas a linear elastic response (EL) was considered in the horizontal direction; this assumption has been shown to be reasonable based on the analysis of tunnelling problems (Basile, 2014). The proposed finite element (FEM) model was developed for groups of vertical piles of length L_p, diameter d_p, and Young's modulus E with piles being modelled as Euler-Bernoulli beams embedded in a uniform continuum. This paper limits itself to excavation-single pile interaction; elevated caps, raft foundations, and superstructure contribution are neglected by assuming constant pile head loads during excavations. All these aspects can be accommodated within the proposed formulation following Franza *et al.* (2017); Leung *et al.* (2010) and Leung *et al.* (2017).

Considering the above assumptions, starting from the framework of Leung *et al.* (2010) and Franza & DeJong (2019), the FEM model was developed by solving the set of expressions given in Equations (1)-(3). Equation (1) is the equilibrium equation; Equation (2) describes the near-pile stiffness; Equation (3) accounts for the sliders. The fully linear elastic solution (EL) is obtained from Equations (1) and (2) while assuming $R_f = 0$; the elastic perfectly-plastic solution (EP) results from Equations (1)-(3) imposing $R_f = 0$; and the nonlinear elastoplastic solution (NEP) is given by Equations (1)-(3) for $R_f \neq 0$.

$$\left(\mathbf{S} + \mathbf{K}^*\right)\mathbf{u} = \mathbf{p} + \mathbf{K}^*\mathbf{u}^{cat} + \mathbf{K}^*\mathbf{\Lambda}^*\left\langle \mathbf{f} \right\rangle + \mathbf{K}^*\mathbf{u}^{ip}; \mathbf{f} = \left(\mathbf{p} - \mathbf{S}\mathbf{u}\right) \tag{1}$$

$$\mathbf{K}^* = \mathbf{R}\left(\mathbf{\Lambda} - \mathbf{\Lambda}^*\right)^{-1}; \qquad R_{ii} = \begin{cases} 1, & \text{for unloading} \\ \left(1 - R_f \dfrac{f_i}{f_{f,i,down}}\right)^2, & \text{for loading} \\ \left(1 - R_f \dfrac{f_i}{f_{f,i,up}}\right)^2, & \text{for reverse loading} \end{cases} \tag{2}$$

$$\left\langle \mathbf{f} \right\rangle_i = f_{f,i,up} < \left(\mathbf{P} - \mathbf{S}\mathbf{u}\right)_i < f_{f,i,down} \tag{3}$$

where $\mathbf{u}$ is the displacement vector of the pile (consisting of three translational and three rotational degrees of freedom), $\mathbf{p}$ is the external loading vector at the pile head, $\mathbf{f}$ is the vector of forces applied by the foundation nodes to the soil (i.e. a vector containing the forces acting on the soil medium), $\mathbf{S}$ is the stiffness matrix of the pile foundation, $\mathbf{u}^{ip}$ is the plastic slider displacement vector, $\mathbf{u}^{cat}$ is the greenfield ground displacement vector, $\mathbf{\Lambda}$ is the linear elastic soil flexibility matrix relating the soil displacement field to the point of application of a force, $\mathbf{\Lambda}^*$ is the non-diagonal term of $\mathbf{\Lambda}$ (i.e. soil flexibility matrix without the main diagonal), and $\mathbf{K}^*$ is the local (near-pile) stiffness matrix of the soil (i.e. for no stiffness degradation, it is the inverse matrix of the diagonal term of $\mathbf{\Lambda}$ for the linear elastic behaviour in the near-pile soil). The terms $f_{f,i,up}$ (negative) and $f_{f,i,down}$ (positive) are the nodal limit forces for pile uplift and down-drag relative to the soil, which are given by the integration of the ultimate base, $q_{b,f}$, and shaft, τ_f, stresses while considering no tensile capacity at

the pile base. $\mathbf{R}$ is the near-pile stiffness reduction matrix, resulting in the initial linear elastic stiffness during unloading and hyperbolic stiffness degradation for loading and reverse loading. In the NEP solutions, unless stated otherwise, the values $R_f = 1$ for the coefficient of hyperbolic near-pile soil stiffness degradation was used to be consistent with Korff *et al.* (2016).

The EL equations can be solved directly, whereas the EP and NEP expressions require an incremental and iterative procedure. Firstly, the equilibrium equation is solved for incremental variations of the load vector $\mathbf{p}$ while $\mathbf{u}^{cat} = 0$. Secondly, for a constant load $\mathbf{p}$, greenfield settlements $\mathbf{u}^{cat}$ are incrementally applied. Excavation-induced effects (movements and forces) are given by the difference between the variables measured at the end of the first and second stage.

MODEL VALIDATION

To verify the developed EP model, results are compared against data from Basile (2014) for tunnelling adjacent to a single pile, which were obtained using the BEM PGROUPN program for perfectly-plastic soil behaviour with $R_f = 0$. A pile with $L_p = 25$m, $d_p = 0.5$m, and $E = 30$GPa was affected by vertical and horizontal ground movements induced by a 6m diameter tunnel with a depth to axis level of 20m and a horizontal offset from the tunnel centreline to the pile axis of 4.5m. In this validation section, greenfield movements were estimated using the semi-analytical expressions of Loganathan & Poulos (1998), with no external loads applied at the pile head, similar to Basile (2014). The considered soil was clay with $E_{s,0} = 24$MPa and $\nu_s = 0.5$, while the ultimate base and shaft resistances were given by $q_{b,f} = 540$kPa and $\tau_f = 48$kPa (assumed constant along the pile), respectively.

Figure 4 compares the results from the developed EP analysis method (tunnelling-induced pile displacements, deflections, axial forces, and bending moments) with the elastoplastic BEM PGROUPN results from Basile (2014); these outcomes are for an unloaded pile at low and high values of tunnel volume loss, $V_{l,t}$=1 and 5%, respectively. For comparison, greenfield (GF) input movements are also shown; and results using the developed elastic EL model are also included for reference (validated in Franza *et al.* (2019b)). The agreement is satisfactory and, importantly, results show that by limiting the shaft friction in the EP solution significantly changes the EL results (i.e. tunnelling-induced settlements increased and axial forces decreased).

TUNNELLING BENEATH PILES - INFLUENCE OF PARAMETERS

To investigate the combined effects of the pile working conditions and the hyperbolic coefficient of stiffness degradation, the pile and soil considered in the previous section ($L_p = 25$m, $d_p = 0.5$m, $Q_{tot} = 1.99$MN) was subjected to tunnelling from a 6m diameter tunnel at a depth to axis level of 30m. The tunnel is assumed to be located either directly beneath the pile or at tunnel-pile offset of 15m. The greenfield inputs were again computed using Loganathan & Poulos (1998).

Results of tunnelling-induced (Tun.ind.) settlements and forces as well as post-tunnelling (Post-tun.; i.e. the combined effects of initial pile loading and tunnelling-induced actions) pile axial force profiles are reported in Figures 5 and 6 for $SF_0 = 2; 100$ and $R_f = 0; 0.75; 1$. Figure 5 shows outcomes for the offset pile for which greenfield settlements mostly decrease with depth, whereas Figure 6 displays the response of the pile directly above the tunnel where greenfield movements increase with depth. Note that pre-tunnelling axial forces are negligible for $SF_0 = 100$, hence post-tunnelling and tunnelling-induced forces match for this case. In addition, consider than tensile pile axial forces are positive in this paper.

For both tunnel offsets, the reduction in initial pile safety factor SF_0, associated with a greater pile head load, resulted in a slight increase in pile settlement, a reduction of the magnitude of tunnelling-induced forces, and a change in the shape of the axial force profile; these trends agree with conclusions of Williamson *et al.* (2017b). Figures 5 and 6 illustrate that the impact of the hyperbolic coefficient R_f on tunnelling-induced displacements is minor, though higher values of R_f tend to slightly reduce tunnelling-induced forces; this latter trend is reasonable considering the near-pile soil stiffness degradation associated with R_f.

Most of the tunnelling-induced forces in Figure 5 are compressive because the offset pile was subjected to greenfield settlements that decrease with depth. On the other hand, greenfield settlements that increase with depth can result in tensile forces due to tunnelling, as shown in Figure 6. However, Figure 6 indicates that the entire pile undergoes tensile post-tunnelling forces for $SF_0 = 100$ (see Figure 6d), whereas only the bottom part of the pile is under tension when $SF_0 = 2$ (see Figure 6c). Interestingly, the largest tensile critical force N_c decreases in magnitude with the pile load P (i.e. when SF_0 is reduced), whereas its location is closer to the pile tip for the highly loaded pile ($SF_0 = 2$) than the lightly loaded pile ($SF_0 = 100$).

In the following section, pile settlements and post-tunnelling tensile forces are investigated by assuming linearly increasing/decreasing settlements with depth.

PARAMETRIC RESULTS

Studied scenarios

The NEP analyses in this section consider single piles of length $L_p = 5; 20$m, diameter $d_p = 0.5$m, and Young's modulus E sufficiently large to simulate a rigid pile in a homogeneous soil with a Young's modulus $E_{s,0} = 24$MPa and a Poisson's ratio $\nu_s = 0.5$. The effect of pile compressibility on the considered interaction problem is minor for most practical scenarios, and the hyperbolic coefficient may be set to $R_f = 1$ (Korff *et al.*, 2016). Analyses were conducted using greenfield settlements that linearly increase or decrease with depth z, as shown in Figure 2, which can approximate excavation-induced settlements (e.g. Williamson *et al.* (2017b); Korff *et al.* (2016)).

Both purely-frictional and floating piles (labelled *FR* and *FL*, respectively) were considered with $q_{b,f}$ either null or proportional to τ_f at the pile base. In this way, purely-frictional and floating piles are defined with respect to the mobilised reaction stresses for extremely large pile settlements. Two possible τ_f profiles along the pile axis were modelled: a constant (e.g. *FR.con*) and linearly increasing (e.g. *FR.inc*) profile of τ_f with z. In addition, to consider low shaft capacity piles due to interface disturbance or shaft coating, an additional analysis was performed for a coated pile with a reduced constant τ_f (*CO.con*). A summary of the considered cases is given in Table 1, where the first three scenarios are used as the 'main analyses' to demonstrate the salient features of the analysis results, and the outcomes of the remaining scenarios are included as supplemental data.

In this work, the ultimate capacity Q_{tot} and the pile safety factor SF_0 are defined based on the very large pile settlements, potentially greater than $10\%d_p$, needed to fully mobilise both τ_f and $q_{b,f}$, as shown in Figure 7a. Engineering judgement should be applied in specific scenarios to assess Q_{tot}. Therefore, use of the proposed design charts presented later is predicated on the existence of data which enables estimation of Q_{tot} and SF_0 for very large pile settlements (i.e. pile settlement of at least $10\%d_p$). Furthermore, Figures 7b and 7c sketch the pre-excavation loading sequence for non-displacement (NP; path A→B) and displacement (DP; path A→D) piles.

In the parametric study presented here, $u_{z,gf}$ is modelled only in terms of ΔS, which is the differential greenfield settlement between the surface and pile base. The surface greenfield settlement ($u_{z,gf,0}$, labelled S_0 here for consistency with Korff *et al.* (2016)) is $S_0 = 0$ in the performed analyses because a) the tunnel-pile interaction problem only depends on ΔS, and b) a uniform greenfield settlement profile due to S_0 results in a pile settlement that is simply equal to the soil settlement, with no variation in the pile axial forces. For instance, from the definition of the interaction level depth, the excavation-induced pile settlement is $u_{pile} = S_0 - z_i/L_p \times \Delta S$, whereas z_c and N_c are not dependent on S_0.

Similar to Korff *et al.* (2016), low and high levels of greenfield settlements were considered by analysing $u_{z,gf}$ characterised by a ratio $\Delta S/D_z = -10, -1, 1, 10$, where ΔS is the difference between greenfield displacement at the pile head and base (defined in Figure 2) and $D_z = Q_{tot}/K_0$ is the ratio between the total pile capacity and the initial stiffness of the load-settlement curve (illustrated in Figure 7a). For instance, a negative value of ΔS relates to piles above the tunnel where greenfield settlements increase with depth, whereas a positive ΔS relates to piles relatively far from the tunnel or adjacent to deep excavations, where greenfield settlements decrease with depth. On the other hand, the parameter D_z is defined for the non-linear analysis (NEP) as the displacement obtained from the pile load-settlement curve $P - u_z$ (for no ground movements) by the intersection between the ultimate capacity Q_{tot} and the tangent to the initial portion of the curve with a slope equal to K_0. Alternatively, D_z would be the settlement corresponding to the full mobilisation of pile capacity from pile loading results in an elastic-perfectly plastic (EP) analysis.

To generalise the outcomes from this work, results are presented using the dimensionless groups in Equation (4) used by Korff *et al.* (2016).

$$SF_0 = \frac{Q_{tot}}{P}, \quad \frac{\Delta S}{D_z}, \quad \frac{\tau_{f,L_p}}{\tau_{f,0}}, \quad Q_r = \frac{Q_b}{Q_{tot}}, \quad \frac{E_s}{E_p}, \quad \frac{L}{d_p}, \quad \frac{D_z}{d_p} \tag{4}$$

However, similar to Korff *et al.* (2016), the impact of D_z/d_p was neglected (analyses for floating piles indicated that it had a minor impact on results), while the ratio $E_s/E_p \approx 0$ for the considered case of a relatively rigid pile. Because of the limited impact of the pile length-to-diameter ratio L/d_p, results presented here focus on the response of relatively long floating piles with $L/d_p = 40$. Within this dimensionless representation, results for the floating piles FL (labelled as Qr05.con, Qr08.inc, and Qr40.con, where the numbers refer to the value of Q_r, i.e. the base capacity as a percentage of the total capacity) provide a description of the variability of all considered cases. Outcomes of the analyses for the remaining scenarios considering both $L/d_p = 10$ and 40 are given in the supplemental data, where the 'supplemental label' in Table 1 is used to refer to each scenario.

Parametric study and dimensionless charts

Firstly, pile settlements relative to the greenfield movements are considered. The normalised interaction level z_i/L_p is plotted against safety factor SF_0 in Figure 8. Engineers are familiar with analysing the relationship between pile and

surface greenfield movements (see Figure 1); thus, the ratios $u_{pile}/u_{gf,0}$ inferred from the data in Figure 8 are plotted in Figure 9 by assuming that $S_0 = u_{gf,0} = 10D_z$. Subsequently, using the same layout, the normalised critical depth z_c/L_p and the ratio between critical axial forces and pull-out pile capacity N_c/Q_t (positive sign assumed for tensile axial forces) are shown in Figures 10 and 11, respectively. Q_t is mobilised by the reverse loading at the pile shaft, as illustrated in Figure 3; in this paper, identical values of τ_f are used for both loading and reverse loading and, thus, the magnitude of Q_t and Q_s are identical. Dashed and solid lines are used for decreasing (positive ΔS; piles far from the tunnel or adjacent to deep excavations) and increasing (negative ΔS; piles above the tunnel) values of $u_{z,gf}$ with z, respectively. Markers are used to distinguish between the pile installation methods: displacement (DP) and non-displacement (NP).

Results for both DP and NP piles in Figure 8 illustrate some general trends: [a] the variation of interaction level is within $z_i/L_p = 0.4 - 0.8$ for both increasing and decreasing greenfield settlement profiles at high SF_0 (e.g. unloaded piles with $SF_0 \geq 4$); [b] z_i/L_p tends to zero (greenfield surface settlement) and unity (greenfield settlement at pile base level) for low SF_0 for decreasing and increasing greenfield settlements, respectively; and [c] the sensitivity of z_i/L_p to the variation of safety factor is considerable within the range of $SF_0 = 1 - 3$. These trends agree qualitatively with the results of Korff *et al.* (2016) for non-displacement piles and a linearly decreasing $u_{z,gf}$. Importantly, because the largest tunnelling-induced values of $u_{z,gf}$ are generally at the location of the pile base and head for piles with their bases within and outside of the tunnel influence zone, respectively, the data in Figure 8 allow for a rational description of the empirical influence zones given by Selemetas (2005) and Kaalberg *et al.* (2005) (see Figure 1) while also accounting for soil and pile properties, pile load condition, and pile installation method.

The ratio $u_{pile}/u_{gf,0}$ shown in Figure 9 highlights that pile settlements, normalised by the constant greenfield surface movement, increases with the pile service load P (i.e. for decreasing SF_0) for both linearly increasing and decreasing greenfield movements. This agrees with centrifuge test outcomes of tunnelling beneath piles in clays, which indicated that the lower the value of SF_0, the greater the pile settlement, regardless of the offset of the pile from the tunnel (Williamson *et al.*, 2017b). However, Figure 9 illustrates that the influence of SF_0 on $u_{pile}/u_{gf,0}$ is significant only for steep greenfield movements with $\Delta S_o \approx S_0$, whereas the ratio $u_{pile}/u_{gf,0}$ is about unity when $\Delta S_o << S_0$. For the cases of $|\Delta S| = 10$, the variation of $u_{pile}/u_{gf,0}$ is most significant within the range of $SF_0 \leq 3$, as was the case for the interaction level z_i/L_p.

In Figure 8, the linearly increasing τ_f resulting in $\tau_{f,L_p}/\tau_{f,0} = 3$ (QR08.inc) contributed to a slight increase in the value of z_i/L_p (i.e. towards the pile base) compared to a constant τ_f associated with $\tau_{f,L_p}/\tau_{f,0} = 1$ (Qr05.con). Similarly, the effects of $\tau_{f,L_p}/\tau_{f,0}$ on $u_{pile}/u_{gf,0}$, normalised critical depth z_c/L_p, and axial force N_c/Q_t is shown to be minor in Figures 9, 10, and 11. Thus, the overall impact of $\tau_{f,L_p}/\tau_{f,0}$ is secondary compared to the other dimensionless parameters within the investigated ranges.

With respect to the base capacity of the DP and NP piles with varying $Q_r = Q_b/Q_{tot}$ (Qr05.con and Qr40.con), the impact of the increase in the relative base capacity is notable: increasing Q_r from 5% to 40% generally shifted z_i/L_p towards the pile base (Figure 9), while it shifted the normalised force N_c/Q_t towards negative (compressive) values for $SF_0 < 3$ (Figure 11). In particular, all considered piles with $Q_r = 40\%$ in Figure 11c are under compression along their entire length for $SF_0 < 2$ ($N_c/Q_c < 0$), hence they would be at a low risk of cracking. This is not the case for the piles in Figure 11a and b subjected to increasing settlement with depth ($\Delta S < 0$), which have low values of Q_r and may undergo tensile values of N_c/Q_t for most values of SF_0. Furthermore, as confirmed by Figures S1-S4 in the supplemental data, results for purely-frictional FR and floating FL piles with $Q_r < 10\%$ are similar, hence the charts for Qr05.con and Qr08.inc are also applicable to purely-frictional FR piles when $Q_b/Q_{tot} < 10\%$.

The location of the critical axial force along the pile is shown in Figure 10 using the normalised critical level depth z_c/L_p. Note that Figure 11 demonstrated that post-excavation tensile forces ($N_c/Q_t > 0$) are limited to the case of increasing greenfield settlements with depth ($\Delta S < 0$); decreasing settlements with depth ($\Delta S > 0$) result in compressive excavation-induced axial forces for all cases ($N_c/Q_t < 0$). Consequently, a critical level depth z_c is not presented for $\Delta S > 0$. Figure 10 shows that z_c moves towards the base of the pile for decreasing SF_0 and reaches $z_c/L_p = 1$ at $SF_0 \approx 1.5$ for all cases (the rate of change is notable between $SF_0 = 1.5$ and 3). Also, in general, the DP values of z_c/L_p are lower (towards the pile head) than for NP for a given value of $\Delta S/D_z$. This is due to the presence of residual (post-loading and pre-excavation) compressive axial forces near the pile mid-depth region for DP piles.

Focusing again on the critical case of $\Delta S < 0$ which can produce tensile axial forces, Figure 11 shows that, as a general trend, the pile critical axial forces N_c/Q_t increase with the settlement rate $\Delta S/D_z$ = -1 → -10, particularly for $SF_0 > 2$. For typical design values of $SF_0 = 2 - 3$, $N_c/Q_t \approx 25\%$, whereas for extremely large values of SF_0, the upper-bound of N_c/Q_t approaches 40%. For low safety factors ($SF_0 < 1.5$), N_c/Q_t values are either close to zero (when $Q_r \approx 0$) or negative (when $Q_r > 0$), while $z_c/L_p = 1$ in these cases. The fact that the pile undergoes no tensile axial forces for low safety factors is in agreement with previous research that indicated negligible variation in pile axial forces due to tunnelling when the service load is close to the total capacity (e.g. Zhang *et al.* (2011a)). This phenomenon occurs because, prior to the ground

movements, the application of a service load P of magnitude approaching the total capacity Q_{tot} mobilises most of the soil capacity and causes a degradation of the near-pile tangent soil stiffness (i.e. the reduction factor R_{ii} is close to zero). Therefore, excavation-induced forces $\mathbf{K}^*\mathbf{u}^{cat}$, which relate to R_{ii}, are negligible in magnitude for very low safety factors, while N_c/Q_t depends mostly on the head load P.

Results in Figures 8, 10, and 11 show that the normalised settlement magnitude $\Delta S/D_z$ affects the relative response, in terms of pile settlement and axial behaviour, of displacement (DP) and non-displacement (NP) piles. The difference between DP and NP outcomes is particularly obvious for $|\Delta S/D_z| = 1$ (except for $SF_0 = 1.1$, which is the lowest considered safety factor), while the response of DP and NP piles is similar for $|\Delta S/D_z| = 10$. The reasons for these trends are summarised as follows.

- Prior to ground movements ΔS, displacement piles DP have an unloading soil stiffness as well as residual stresses. For DP with $SF_0 > 1.5$, the final loading step D is far from the intermediate step B (that mobilised the ultimate capacity) in Figure 7c. For small ground movements ($|\Delta S/D_z| = 1$) the pile responds with its tangent re-loading stiffness equal to $E_{s,0}$ (along the segment B'-A in Figure 3b). Thus, the value of z_i/L_p of the DP pile does not vary much from the average settlement $z_i/L_p \approx 0.5$ that is typical for an elastic EL analysis. However, z_i/L_p shifts towards the pile head or base for greater greenfield movements (see $|\Delta S/D_z| = 10$) because the soil transitions from the re-loading stiffness to the further loading stiffness (A-B in Figure 3b, where tangent stiffness E is given by E_s reduced by R_{ii}) and pile settlements approach maximum greenfield settlements (z_i/L_p tends to 0 or 1) rather than the average settlement ($z_i/L_p \approx 0.5$).

- For DP piles with $SF_0 = 1.1$ (the lowest considered safety factor), the response is close to NP behaviour because the final loading step D is close to the intermediate step B that mobilised the ultimate capacity. Thus, the range of high re-loading stiffness (along the segment B'-A in Figure 3b) is rather small and the state of further loading (A-B in Figure 3b) is reached for low values of greenfield ground movements.

- For both NP and DP piles with large values of $|\Delta S/D_z| = 10$, the excavation-induced relative soil-pile displacements dominate and, thus, the pile loading path prior to excavation has little effect.

Example application of design charts

To illustrate the use of the proposed design charts, the case Qr05.con of a floating non-displacement pile ($d_p = 0.5$m, $L = 20$m) embedded in a uniform ground with a representative initial stiffness $E_{s,0} = 24$MPa and undrained shear strength of 60kPa is considered. From the geometry and soil strength parameters it is estimated that $\tau_f = 60$kPa, $q_{b,f} = 540$kPa, $Q_b = 0.11$MN, $Q_t \approx Q_s = 1.88$MN, and $Q_{tot} = 1.99$MN. The value of $D_z = 9$mm is inferred from Q_{tot}, L/d_p and E_s. If an elastic soil-pile interaction model is not available, engineers may estimate D_z from the load Q_{tot} and the displacement influence factor charts of Poulos & Davis (1968).

The pile is subjected to a linearly increasing profile of greenfield settlements where settlement at the pile head and tip are, respectively, 12 and 21mm; therefore, $S_0 = 12$mm and $\Delta S = -9$mm. The main dimensionless groups representative of the given scenario are $Q_r = 5\%$, SF_0, $\tau_{f,L_p}/\tau_{f,0} = 1, \Delta S/D_z = -1$.

To estimate pile settlement, depth, and magnitude of post-tunnelling critical tensile forces, the solid red (lighter shade in greyscale) curves with no markers in Figures 8-11 are used. First, consider a pile head load of $P = 664$kN, for which $SF_0 = 3$. Using this, the charts give $z_i/L_p = 0.65$, $z_c/L_p = 0.83$, and $N_c/Q_t = 0.025$. Thus, the pile settlement is $u_{pile} = S_0 - z_i/L_p \times \Delta S = 17.9$mm; the normalised critical depth is $z_c = 0.83 \times L_p = 16.6$m; and the maximum post-tunnelling tensile force is $N_c = 0.025 \times Q_t = 47$kN. Second, consider an unloaded pile ($SF_0 \approx 100$) for which $z_i/L_p = 0.53$, $z_c/L_p = 0.55$, $N_c/Q_t = 0.145$. It follows that pile settlement is $u_{pile} = 16.8$mm, normalised critical depth is $z_c = 11$m, and maximum post-tunnelling tensile force is $N_c = 273$kN.

CONCLUSIONS

In this paper, a nonlinear two-stage continuum-based finite element model was proposed to study the problem of tunnel- and deep excavation-pile interaction. A hyperbolic soil model for the near-pile stiffness degradation was incorporated that also considers the effects of pile unloading. The model was validated against boundary element method results based on an assumed elastic perfectly-plastic soil behaviour. Pile ultimate capacity was defined based on predicted loads required for extremely large pile settlements.

Analyses were carried out to evaluate the settlements and internal forces of purely-frictional and floating piles in a uniform ground for different levels of greenfield ground settlements. Greenfield settlements that increase linearly with depth were used to replicate piles located above tunnels, whereas linearly decreasing greenfield settlements were used for piles more distant from the tunnel or adjacent to a deep excavation. The following provides a summary of the main outcomes of the research, where the term excavation is used to imply both tunnels and deep excavations.

- Results illustrated the way in which pile safety factor can increase or decrease excavation-induced pile settlements and tensile forces (the latter only for the case of greenfield settlements increasing with depth), confirming the results of previous works characterised by nonlinear trends due to the interaction mechanisms. On the other hand, for this nonlinear soil-pile interaction model, it was shown that the installation method can significantly affect the axial pile response to ground movements, but only for low levels of excavation-induced settlements.

- The obtained variability of the interaction level (depth at which the affected pile settlement matches the greenfield value) and critical level (depth at which the maximum post-tunnelling tensile axial force occurs) was extremely wide for both purely-frictional and floating piles. For standard design working loads and unloaded piles, the computed maximum values of tensile post-tunnelling axial forces were 25% and 40% of the pull-out (shaft) pile capacity, respectively.

- The nonlinear soil-pile interaction model results are suggested for preliminary design evaluations. Dimensionless charts were provided to allow designers to estimate both settlements and critical (tensile) axial forces of piles affected by excavations, hence providing the first attempt to provide a rational framework that characterises both displacements and internal forces for piles affected by tunnels and deep excavations. The charts account for the normalised greenfield settlement level (high and low); relative base capacity (between zero and 40% of the total capacity); ultimate shaft friction (constant and linearly increasing with depth); pile safety factor (between 1 and 100), and installation method (displacement and non-displacement piles). In particular, the proposed charts are more comprehensive than empirical influence zones available in the literature (Kaalberg *et al.*, 2005; Selemetas, 2005), which relate only to the pile base-to-tunnel relative location and do not provide quantitative insights as to the effect of excavations on piles. Furthermore, in agreement with Korff *et al.* (2016), results demonstrate that available empirical methods which assume that the interaction level occurs at the surface or at two-thirds of the pile length (for purely-frictional and floating piles, respectively) may be misleading. Finally, note that these design charts are applicable only for elastic pile behaviour; if a pile is susceptible to cracking and softening, then the charts can only be applied up to a state associated with pile cracking.

Finally, the proposed simplified model has limitations, particularly for predicting the response of displacement piles. Note that this paper dealt with the effects of ground movements while neglecting the impact of effective stress variations (due to the excavations or from pile installation), which can alter the tunnel-pile interactions, particularly for displacement piles in sand (Marshall & Mair, 2011). Further work is also needed to better characterise the effects of tunnelling while considering installation processes (e.g. driven, jacked, screwed piles), and pile tip geometry (e.g. open/closed-ended).

ACKNOWLEDGEMENTS

This project has received funding from the European Union's Horizon 2020 research and innovation programme under the Marie Sklodowska-Curie grant agreement No 793715.

SUPPLEMENTAL DATA

Figures S1-S4 are available online [link will be added].

NOTATION

d_p	pile diameter
$f_{f,i,down}$	limit force in relative down-drag
$f_{f,i,up}$	limit force in relative uplift
ν_s	Poisson's ratio for soil
$q_{b,f}$	base ultimate stress
τ_f	shaft ultimate stress
u_z	vertical displacement
$u_{z,max}$	maximum vertical displacement
$u_{z,gf}$	greenfield settlement
$u_{z,gf,0}$	greenfield surface settlement
u_{pile}	pile settlement
z_c	critical level depth
z	depth, measured from ground surface
z_i	interaction level depth
z_t	depth of tunnel axis
ΔS	differential greenfield settlement between surface and pile base
D_z	relative displacement between soil and pile at failure for an elastic perfectly-plastic soil behaviour
E_p	Young's modulus of pile
E_s	Young's modulus of soil
$E_{s,0}$	initial Young's modulus of soil
K_0	initial stiffness of the load-settlement curve
Lp	pile length
N_c	critical axial force
P	service head load of pile
Q_b	ultimate capacity of pile base
Q_r	pile base capacity as a percentage of total capacity
Q_s	ultimate capacity of pile shaft
Q_t	ultimate pull-out pile capacity
Q_{tot}	maximum capacity of pile;
R_f	coefficient of hyperbolic stiffness reduction
S_0	greenfield surface settlement
SF_0	safety factor
$V_{l,t}$	volume loss of tunnel
NP	non-displacement pile
DP	displacement pile
$\mathbf{f}$	vector of forces acting on the soil
$\mathbf{p}$	external loading vector
$\mathbf{u}$	pile displacement vector
$\mathbf{u}^{ip}$	slider displacement vector
$\mathbf{u}^{cat}$	greenfield ground displacement vector
$\mathbf{R}$	near-pile stiffness reduction matrix
$\mathbf{S}$	pile stiffness matrix
$\mathbf{\Lambda}$	elastic soil flexibility matrix
$\mathbf{\Lambda}^*$	non-diagonal term of $\mathbf{\Lambda}$
$\mathbf{K}^*$	soil near-pile stiffness matrix

REFERENCES

Basile, F. (2014). Effects of tunnelling on pile foundations. *Soils and Foundations* **54**, No. 3, 280–295, doi:10.1016/j.sandf.2014.04.004.

Bel, J., Branque, D., Wong, H., Viggiani, G. & Losacco, N. (2015). Experimental study on a 1g reduced scale model of TBM: impact of tunnelling on piled structures. In *Proceedings of the XVI European Conference on Soil Mechanics and Geotechnical Engineering, ECSMGE 2015*, pp. 413–418.

Castelli, F. & Maugeri, M. (2002). Simplified Nonlinear Analysis for Settlement Prediction of Pile Groups. *Journal of Geotechnical and Geoenvironmental Engineering* **128**, No. 1, 76–84, doi:10.1061/(ASCE)1090-0241(2002)128:1(76).

Chen, L. T., Poulos, H. G. & Loganathan, N. (1999). Pile responses caused by tunneling. *Journal of Geotechnical and Geoenvironmental Engineering* **125**, No. 2-3, 207–215.

Chow, Y. K. (1986). Analysis of vertically loaded pile groups. *International Journal for Numerical and Analytical Methods in Geomechanics* **10**, No. 1, 59–72, doi:10.1002/nag.1610100105.

Devriendt, M. & Williamson, M. (2011). Validation of methods for assessing tunnelling-induced settlements on piles. *Ground Engineering* , No. March, 25–30.

Dias, T. & Bezuijen, A. (2018). Pile tunnel interaction: Pile settlement vs Ground settlements. In *ITA World Tunnel Congress 2018 - The role of underground space in building future sustainable cities*, Dubai, United Arab Emirates.

Dias, T. G. S. & Bezuijen, A. (2015). Data Analysis of Pile Tunnel Interaction. *Journal of Geotechnical and Geoenvironmental Engineering* **141**, No. 12, 04015051, doi:10.1061/(ASCE)GT.1943-5606.0001350.

Franza, A. & DeJong, M. J. (2019). Elastoplastic solutions to predict tunneling-induced load redistribution and deformation of surface structures. *Journal of Geotechnical and Geoenvironmental Engineering* **145**, No. 4, 04019007, doi:10.1061/(ASCE)GT.1943-5606.0002021.

Franza, A. & Marshall, A. M. (2019). Centrifuge and real-time hybrid testing of tunneling beneath piles and piled buildings. *Journal of Geotechnical and Geoenvironmental Engineering* **145**, No. 3, 04018110, doi:10.1061/(ASCE)GT.1943-5606.0002003.

Franza, A., Marshall, A. M., Haji, T., Abdelatif, A. O., Carbonari, S. & Morici, M. (2017). A simplified elastic analysis of tunnel-piled structure interaction. *Tunnelling and Underground Space Technology* **61**, No. Jan, 104–121, doi:10.1016/j.tust.2016.09.008.

Franza, A., Marshall, A. M. & Jimenez, R. (2019a). An analysis method for the effects of tunnelling on loaded non-displacement piles. In *XVI Panamerican Conference on Soil Mechanics and Geotechnical Engineering*.

Franza, A., Marshall, A. M. & Jimenez, R. (2019b). Elastic analysis of tunnelling beneath capped pile groups. In *Proceedings of the XVII ECSMGE-2019: Geotechnical Engineering foundation of the future*.

Hong, Y., Soomro, M. & Ng, C. (2015). Settlement and load transfer mechanism of pile group due to side-by-side twin tunnelling. *Computers and Geotechnics* **64**, No. March, 105–119, doi:10.1016/j.compgeo.2014.10.007.

Huang, M. & Mu, L. (2012). Vertical response of pile raft foundations subjected to tunneling-induced ground movements in layered soil. *International Journal for Numerical and Analytical Methods in Geomechanics* **36**, No. 8, 977–1001, doi:10.1002/nag.1035.

Jacobsz, S. W., Bowers, K. H., Moss, N. A. & Zanardo, G. (2005). The effects of tunnelling on piled structures on the CTRL. In *Proceedings of the 5th International Conference of TC28 of the ISSMGE on Geotechnical Aspects of Underground Construction in Soft Ground* (Bakker, K. J., Bezuijen, A., Broere, W. & Kwast, E., eds.), Amsterdam, the Netherlands: Balkema, Leiden, Netherlands, pp. 115–121.

Kaalberg, F. J., Teunissen, E. A. H., van Tol, A. F. & Bosch, J. W. (2005). Dutch research on the impact of shield tunnelling on pile foundations. In *Proceedings of the 5th International Conference of TC28 of the ISSMGE on Geotechnical Aspects of Underground Construction in Soft Ground* (Bakker, K. J., Bezuijen, A., Broere, W. & Kwast, E. A., eds.), Amsterdam, the Netherlands: Taylor & Francis - Balkema, pp. 123–131.

Kitiyodom, P., Matsumoto, T. & Kawaguchi, K. (2005). A simplified analysis method for piled raft foundations subjected to ground movements induced by tunnelling. *International Journal for Numerical and Analytical Methods in Geomechanics* **29**, No. 15, 1485–1507, doi:10.1002/nag.469.

Korff, M., Mair, R. J. & Tol, F. A. F. V. (2016). Pile-Soil Interaction and Settlement Effects Induced by Deep Excavations. *Journal of Geotechnical and Geoenvironmental Engineering* **142**, No. 8, 04016034.

Lee, C.-J. J. & Chiang, K.-H. H. (2007). Responses of single piles to tunneling-induced soil movements in sandy ground. *Canadian Geotechnical Journal* **44**, No. 10, 1224–1241, doi:10.1139/T07-050.

Leung, Y. F., Klar, A. & Soga, K. (2010). Theoretical Study on Pile Length Optimization of Pile Groups and Piled Rafts. *Journal of Geotechnical and Geoenvironmental Engineering* **136**, No. 2, 319–330, doi:10.1061/(ASCE)GT.1943-5606.0000206.

Leung, Y. F. A., Klar, A., Soga, K. & Hoult, N. A. (2017). Superstructure-foundation interaction in multi-objective pile group optimization considering settlement response. *Canadian Geotechnical Journal* **54**, No. 10, 1408–1420.

Loganathan, N. & Poulos, H. G. (1998). Analytical prediction for tunneling-induced ground movements in clays. *Journal of Geotechnical and Geoenvironmental Engineering* **124**, No. 9, 846–856, doi:10.1061/(ASCE)1090-0241(1998)124:9(846).

Loganathan, N., Poulos, H. G. & Xu, K. J. (2001). Ground and pile-group responses due to tunnelling. *Soils and Foundations* **41**, No. 1, 57–67.

Mair, R. & Williamson, M. (2014). The influence of tunnelling and deep excavation on piled foundations. In *Proceedings of the 8th International Symposium on Geotechnical Aspects of Underground Construction in Soft Ground* (Yoo, C., Park, S.-W., Kim, B. & Ban, H., eds.), Seoul, South Korea: Taylor and Francis - Balkema, pp. 21–30, doi:10.1201/b17240-6.

Marshall, A. M. A. & Mair, R. R. J. (2011). Tunneling beneath driven or jacked end-bearing piles in sand. *Canadian Geotechnical Journal* **48**, No. 12, 1757–1771, doi:10.1139/t11-067.

Mu, L., Huang, M. & Finno, R. J. (2012). Tunnelling effects on lateral behavior of pile rafts in layered soil. *Tunnelling and Underground Space Technology* **28**, 192–201, doi:10.1016/j.tust.2011.10.010.

Poulos, H. G. (1989). Pile behaviour - theory and application. *Géotechnique* **39**, No. 3, 365–415.

Poulos, H. G. & Chen, L. T. (1997). Pile response due to excavation-induced lateral soil movement. *Journal of Geotechnical and Geoenvironmental Engineering* **123**, No. 2, 94–99, doi:10.1061/(ASCE)1090-0241(1997)123:2(94).

Poulos, H. G. & Davis, E. H. (1968). Settlement behaviour of single axially loaded incompressible piles and piers. *Géotechnique* **18**, No. 3, 351–371.

Selemetas, D. (2005). The response of full-scale piles and piled structures to tunnelling. *Ph.D. Thesis, Cambridge University* .

Selemetas, D. & Standing, J. R. (2017). Response of Full-Scale Piles to EPBM Tunnelling in London Clay. *Géotechnique* **67**, No. 9, 823–836, doi:10.1680/jgeot.SIP17.P.126.

Soomro, M. A., Hong, Y., Ng, C. W. W., Lu, H. & Peng, S. (2015). Load transfer mechanism in pile group due to single tunnel advancement in stiff clay. *Tunnelling and Underground Space Technology* **45**, No. January, 63–72, doi:10.1016/j.tust.2014.08.001.

Soomro, M. A., Mangnejo, D. A., Bhanbhro, R., Memon, N. A. & Memon, M. A. (2019). 3D finite element analysis of pile responses to adjacent excavation in soft clay: Effects of different excavation depths systems relative to a floating pile. *Tunnelling and Underground Space Technology* **86**, No. April, 138–155, doi:10.1016/j.tust.2019.01.012.

Soomro, M. A., Ng, C. W., Liu, K. & Memon, N. A. (2017). Pile responses to side-by-side twin tunnelling in stiff clay: Effects of different tunnel depths relative to pile. *Computers and Geotechnics* **84**, 101–116, doi:10.1016/j.compgeo.2016.11.011.

Williamson, M. G. (2014). Tunnelling effects on bored piles in clay. *Ph.D. Thesis, Cambridge University* .

Williamson, M. G., Elshafie, M. Z. E. B., Mair, R. J. & Devriendt, M. D. (2017a). Open-face tunnelling effects on non-displacement piles in clay - part 1: centrifuge modelling techniques. *Géotechnique* **67**, No. 11, 983–1000, doi:10.1680/jgeot.sip17.P.119.

Williamson, M. G., Mair, R. J., Devriendt, M. D. & Elshafie, M. Z. E. B. (2017b). Open-face tunnelling effects on non-displacement piles in clay - part 2: tunnelling beneath loaded piles and analytical modelling. *Géotechnique* **67**, No. 11, 1001–1019, doi: 10.1680/jgeot.SIP17.P.120.

Zhang, R., Zheng, J., Pu, H. & Zhang, L. (2011a). Analysis of excavation-induced responses of loaded pile foundations considering unloading effect. *Tunnelling and Underground Space Technology* **26**, No. 2, 320–335, doi:http://dx.doi.org/10.1016/j.tust.2010.11.003.

Zhang, R. J., Zheng, J. J. & Yu, S. (2013). Responses of piles subjected to excavation-induced vertical soil movement considering unloading effect and interfacial slip characteristics. *Tunnelling and Underground Space Technology* **36**, 66–79, doi:10.1016/j.tust.2013.02.005.

Zhang, R. J., Zheng, J. J., Zhang, L. M. & Pu, H. F. (2011b). An analysis method for the influence of tunneling on adjacent loaded pile groups with rigid elevated caps. *International Journal for Numerical and Analytical Methods in Geomechanics* **35**, No. 18, 1949–1971, doi:10.1002/nag.

Zhang, Z., Huang, M., Xu, C., Jiang, Y. & Wang, W. (2018). Simplified solution for tunnel-soil-pile interaction in Pasternak's foundation model. *Tunnelling and Underground Space Technology* **78**, 146–158, doi:10.1016/j.tust.2018.04.025.

LIST OF FIGURES

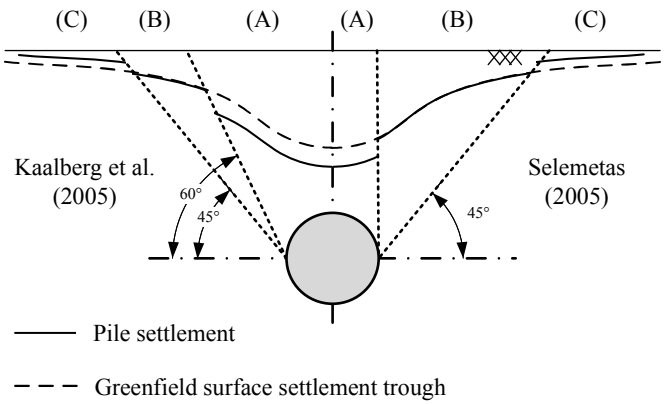

Fig. 1. Relationships between pile and greenfield surface settlements depending on the pile base location (Selemetas, 2005; Kaalberg *et al.*, 2005).

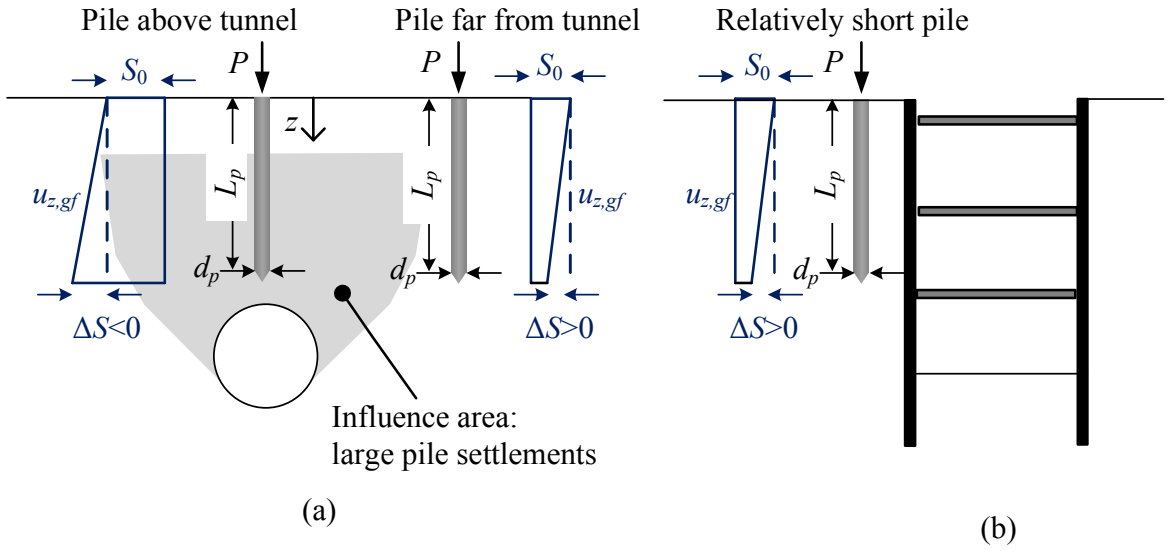

Fig. 2. Sketch of (a) tunnel- and (b) deep excavation-pile interaction problems as well as greenfield ground movement profiles ($u_{z,gf}$) assumed in this work.

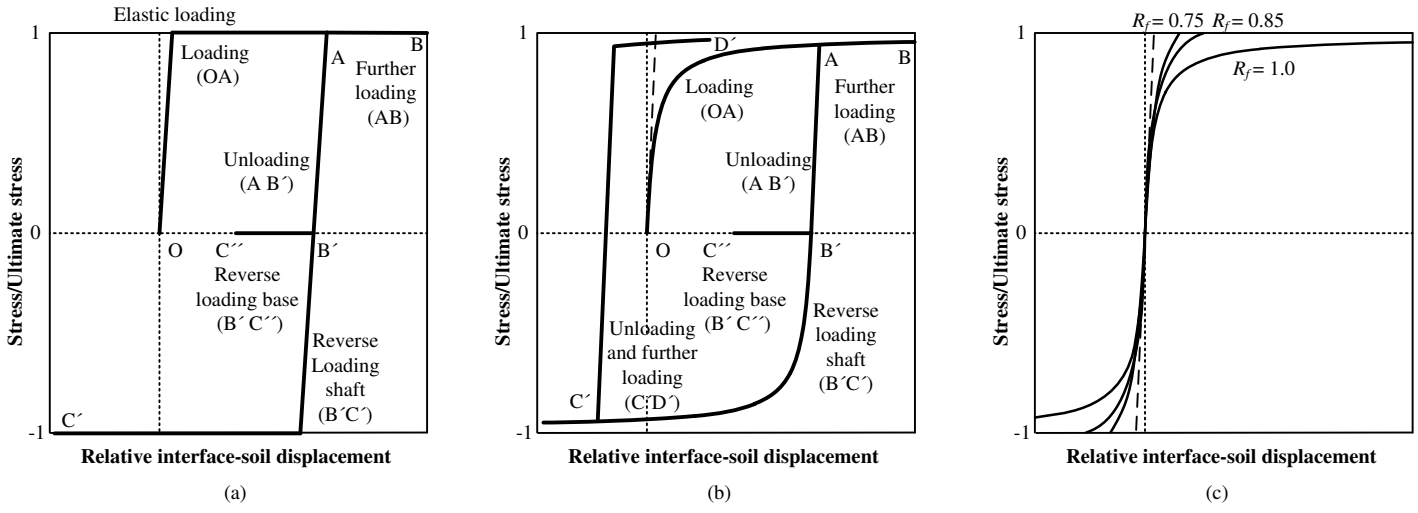

Fig. 3. (a) Linear-elastic perfectly-plastic (EP) and (b) nonlinear elastoplastic (NEP) behaviour of the interface and the near-pile soil for $R_f = 1$ (follow the letter order for loading paths). (c) Influence of coefficient R_f of hyperbolic stiffness reduction.

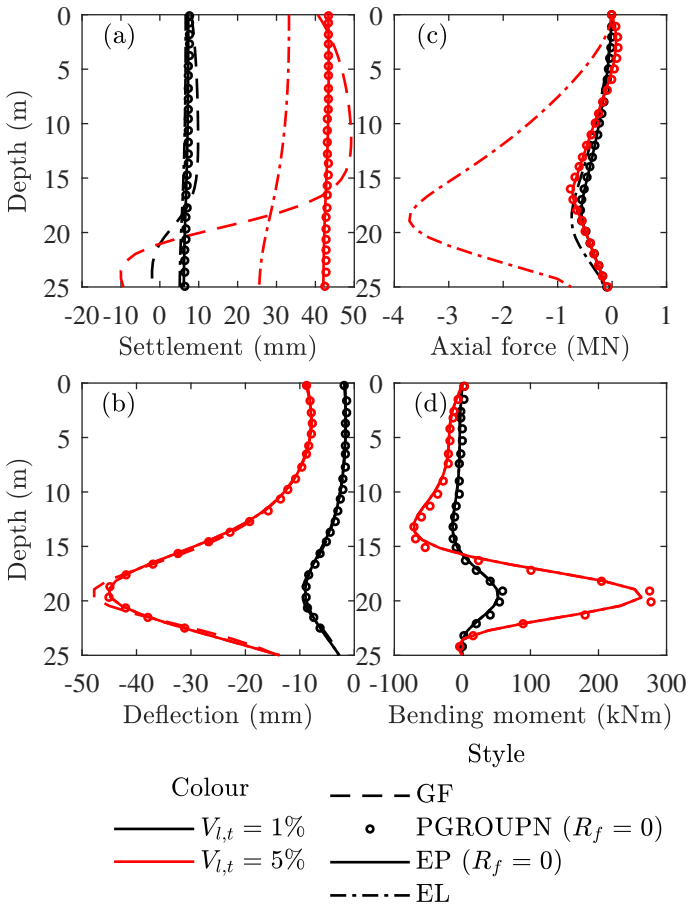

Fig. 4. Tunnelling-induced axial and flexural response of an unloaded single pile.

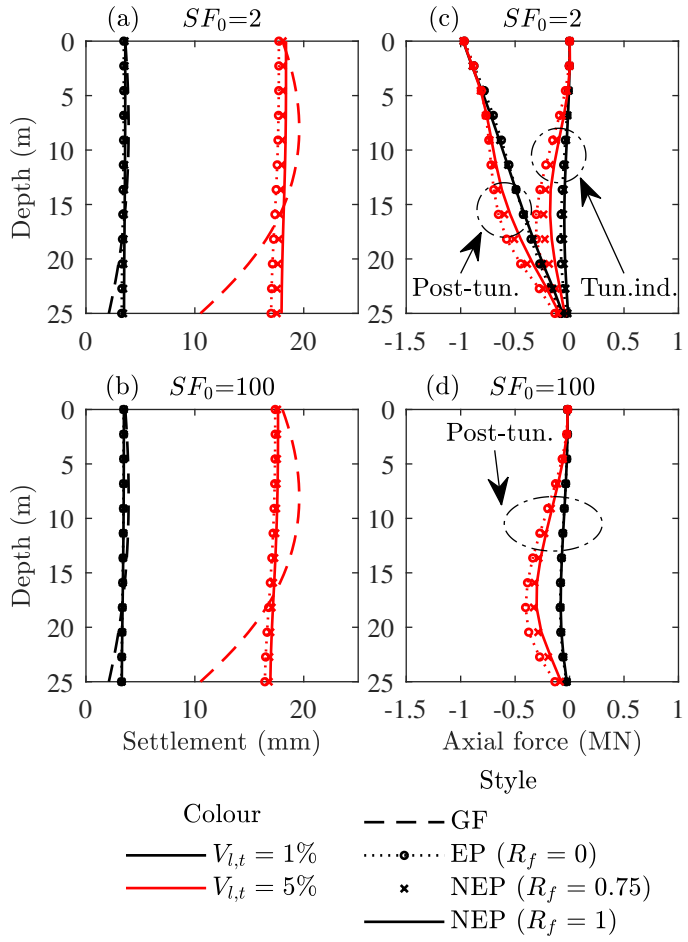

Fig. 5. Axial response for tunnel-pile offset of 15m: (a)-(b) tunnelling-induced settlements; (c)-(d) tunnelling-induced and post-tunnelling force profiles.

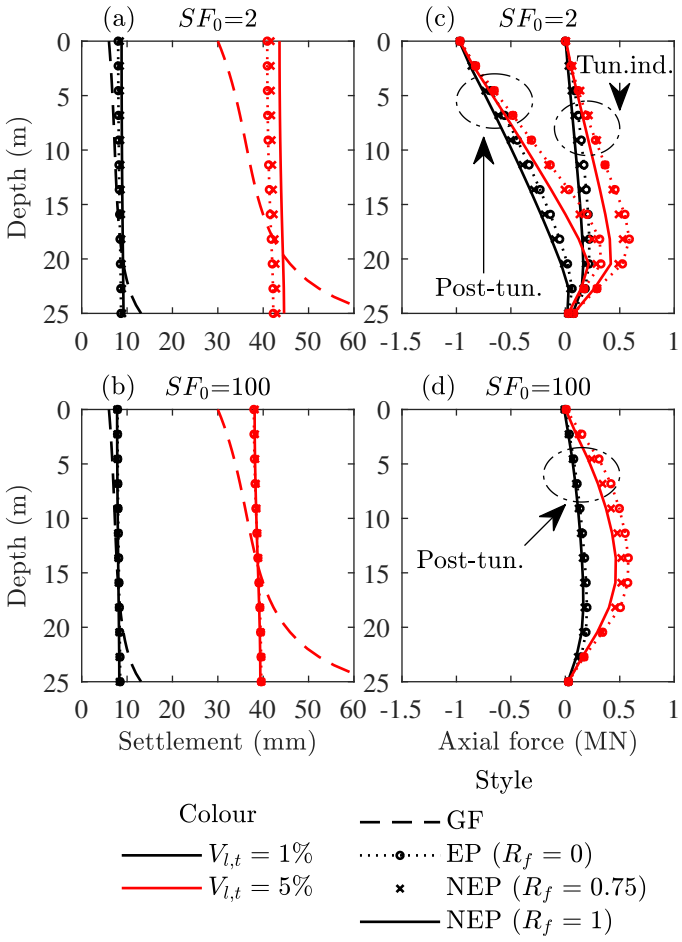

Fig. 6. Axial response for tunnel-pile offset of zero: (a)-(b) tunnelling-induced settlements; (c)-(d) tunnelling-induced and post-tunnelling force profiles.

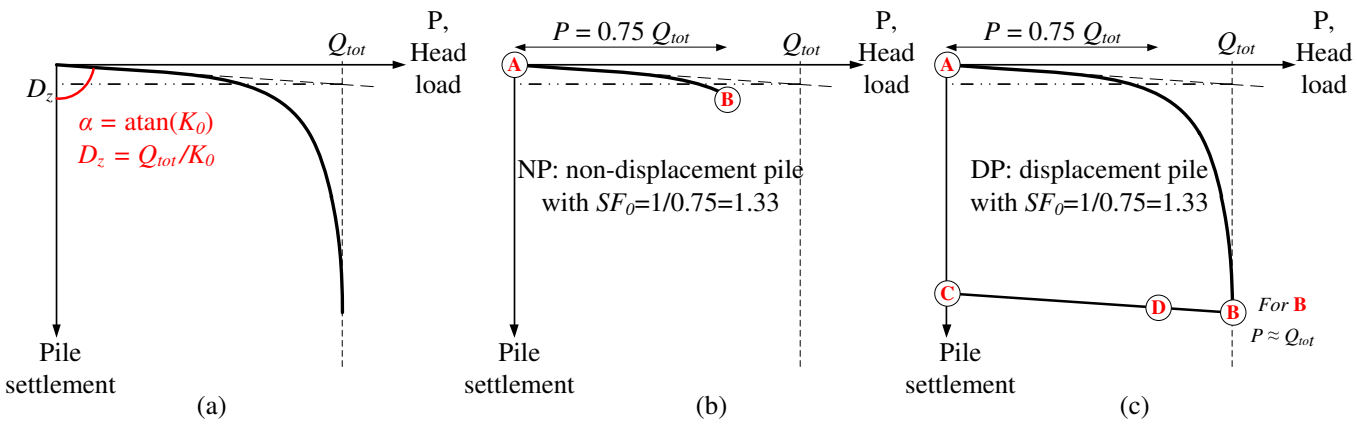

Fig. 7. Conceptual sketches of pre-tunnelling pile loading: (a) pile head load-settlement curve and the definition of the settlement D_z; pre-excavation loading sequence of (b) non-displacement and (c) displacement piles.

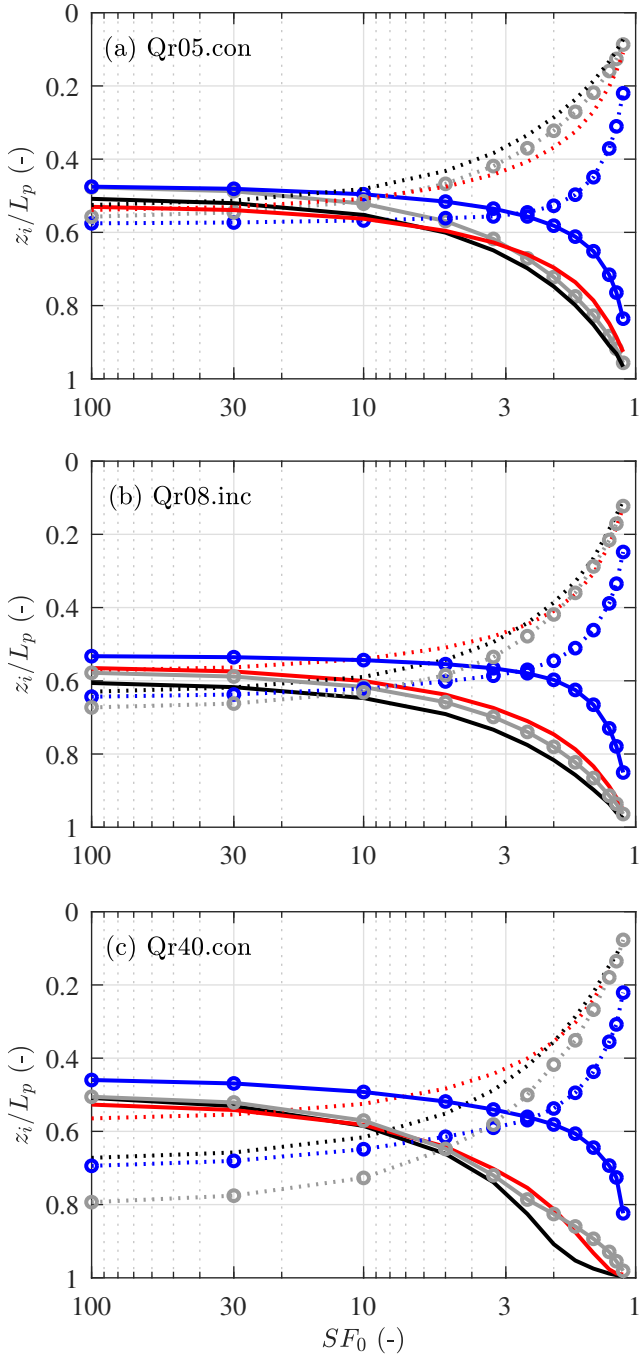

Fig. 8. Normalised interaction level depth (z_i/L_p) for varying pile safety factor and greenfield profiles.

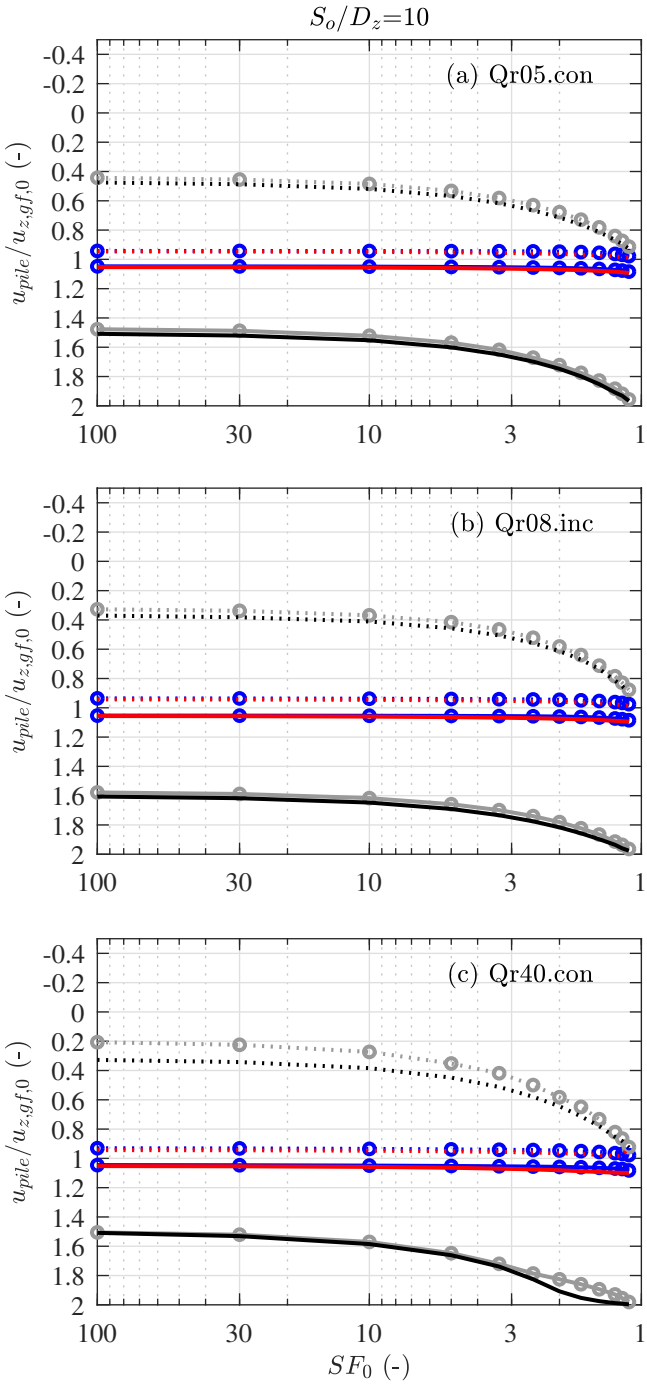

Fig. 9. Ratio between pile and greenfield surface settlements: inferred from Figure 8 by assuming $S_0 = 10D_z$.

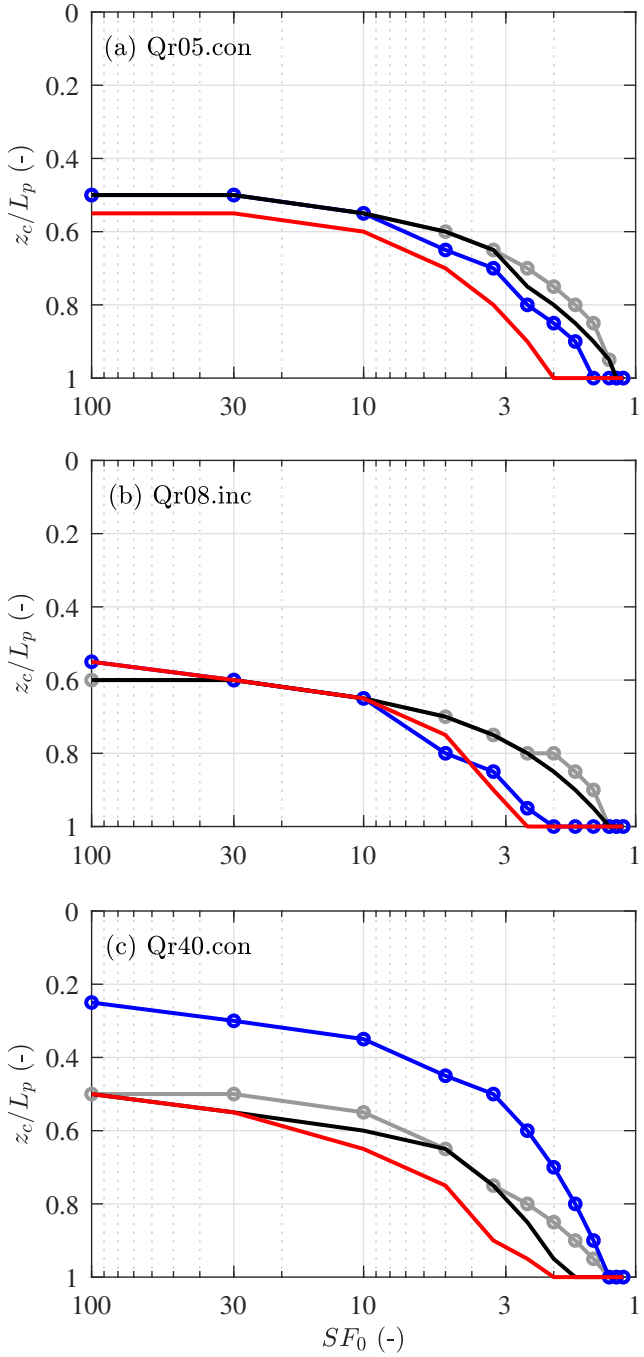

Fig. 10. Critical level depth (z_c/L_p).

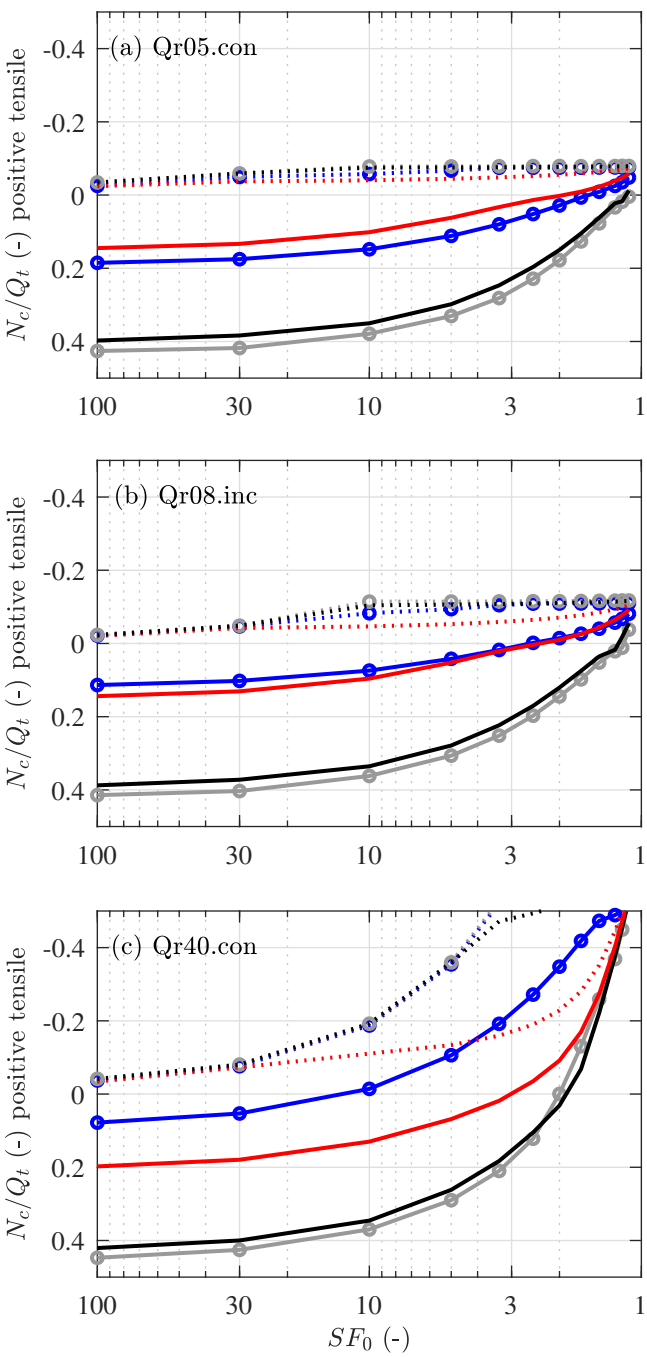

Fig. 11. Post-tunnelling critical axial force (N_c/Q_t).

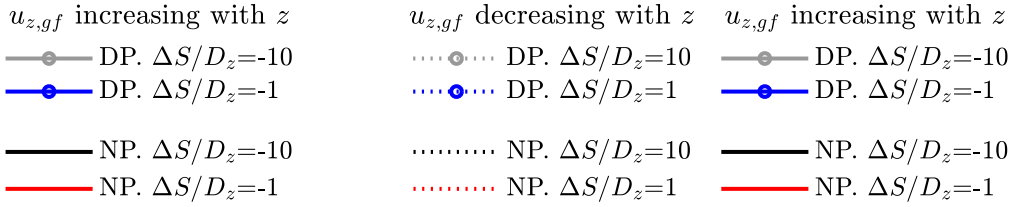

LIST OF TABLES

Table 1. Considered scenarios: main analyses (top half) and supplemental analyses (bottom half).

Label	d_p (m)	L/d_p (−)	$\tau_f(0)$ (kPa)	$\tau_f(L_p)$ (kPa)	$q_{b,f}$ (kPa)	D_z (mm)	$\frac{\tau_f(L_p)}{\tau_f(0)}$ (−)	$Q_r = \frac{Q_b}{Q_{tot}}$ (−)	Supplemental Label
Qr05.con	0.5	40	60	60	9×60	9.0	1	5%	FL.LD40.con
Qr08.inc	0.5	40	30	90	9×90	9.7	3	8%	FL.LD40.inc
Qr40.con	0.5	40	5	5	9×60	1.3	1	40%	CO.LD40.con
	0.5	40	60	60	0	9.0	1	0%	FR.LD40.con
	0.5	40	30	90	0	9.4	3	0%	FR.LD40.inc
	0.5	10	60	60	9×60	6.0	1	0%	FR.LD10.con
	0.5	10	60	60	9×60	7.4	1	18%	FL.LD10.con

LIST OF FIGURES

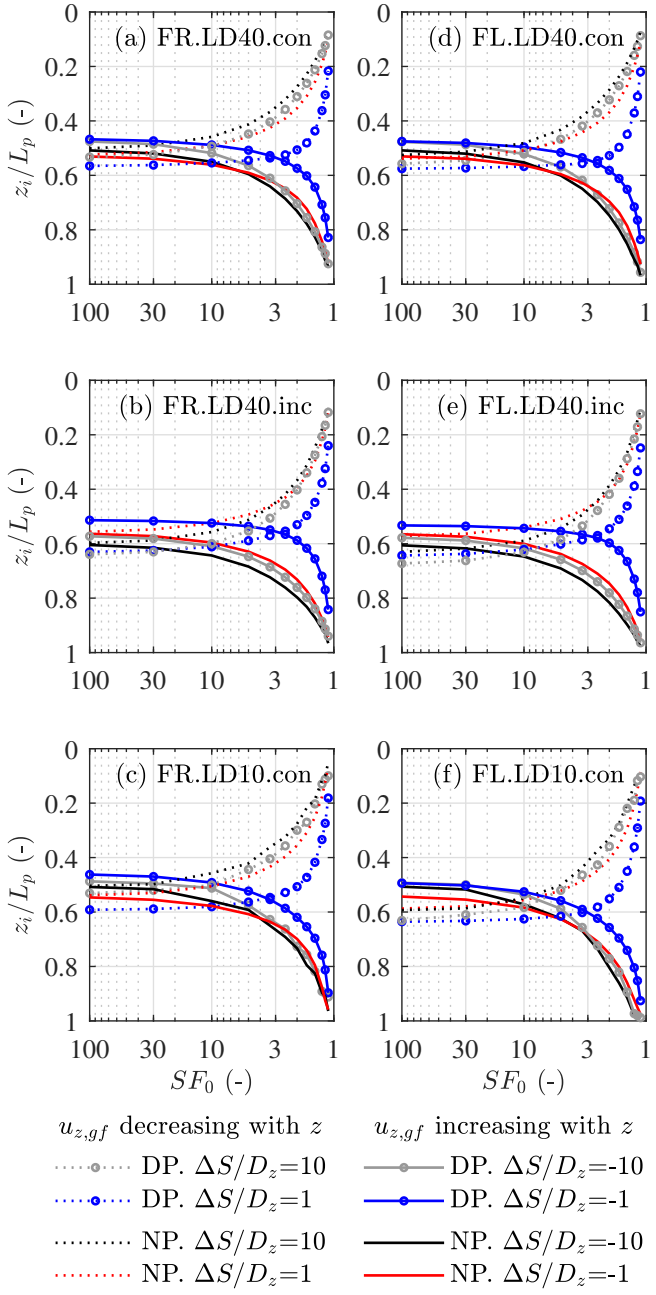

Fig. S1. [Supplemental data] Normalised interaction level depth (z_i/L_p).

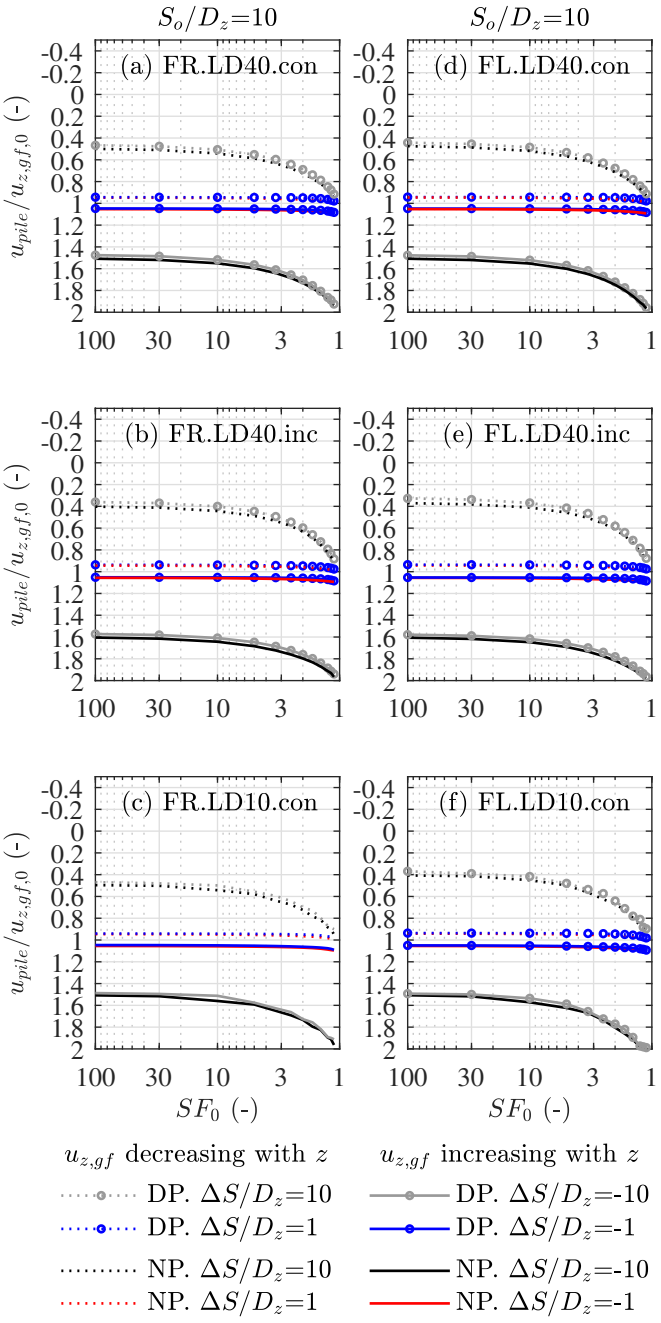

Fig. S2. [Supplemental data] Ratio between pile and greenfield surface settlements.

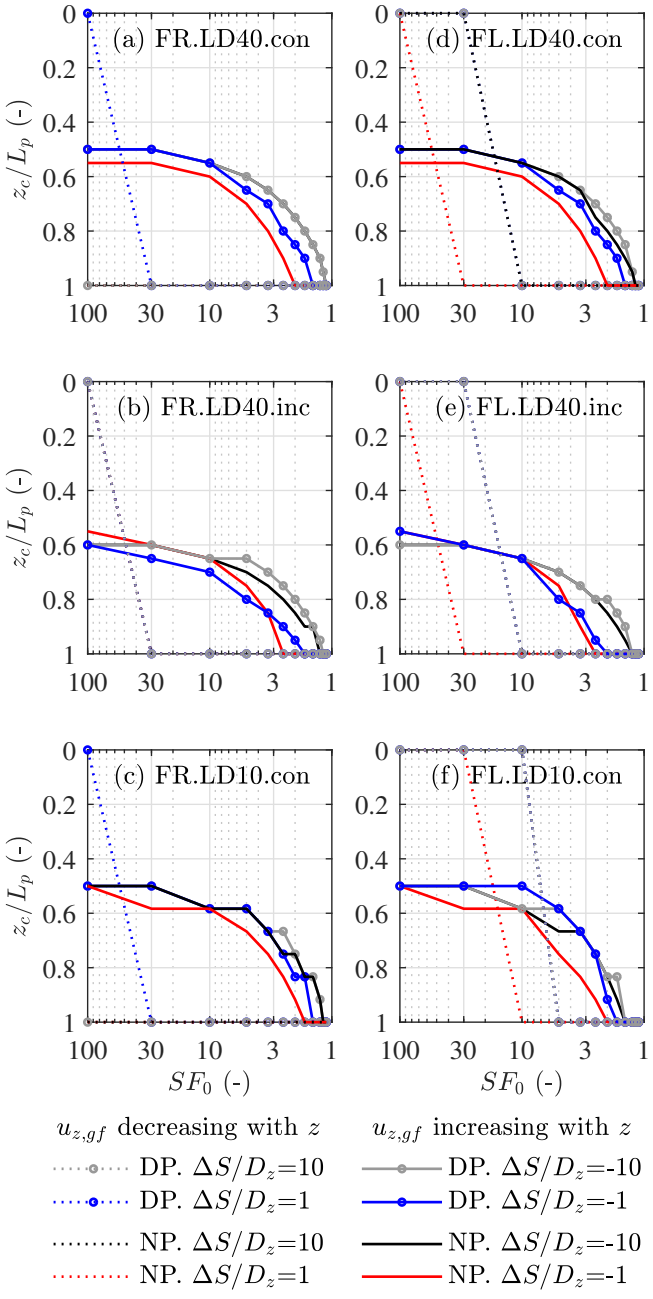

Fig. S3. [Supplemental data] Critical level depth (z_c/L_p).

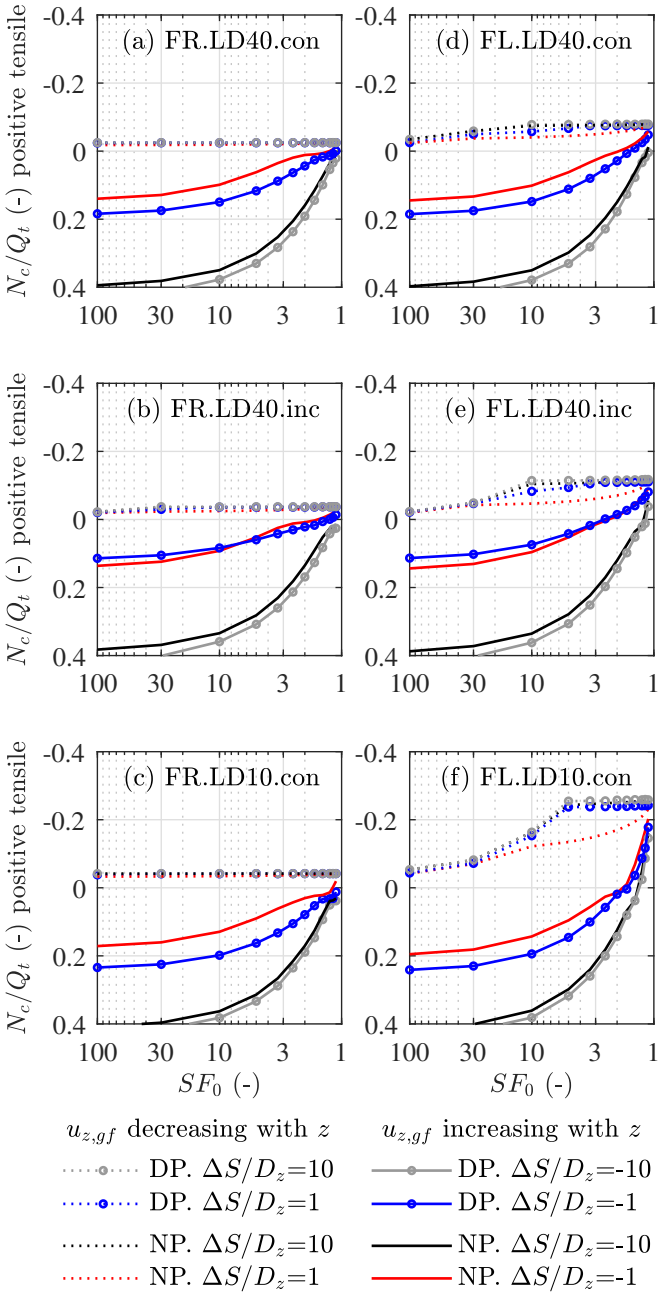

Fig. S4. [Supplemental data] Post-tunnelling critical axial force (N_c/Q_t).